Reaction of the OH Radical with Furfural. Spectral and Kinetic Investigation by Pulse Radiolysis and by ab Initio and Semiempirical Methods

Mila D'Angelantonio,[†] Salvatore S. Emmi,*[,†] Gabriella Poggi,[‡] and Giancarlo Beggiato[†]

Istituto di Fotochimica e Radiazioni d'Alta Energia (FRAE) del CNR, Area della Ricerca, Via P. Gobetti 101, I-40129 Bologna, Italy, and Dipartimento di Chimica "G. Ciamician", Università di Bologna, Via G. Selmi 2, I-40126 Bologna, Italy

Received: September 24, 1998; In Final Form: November 17, 1998

The reaction between the OH radical and furfural and the first stages of the subsequent processes have been investigated in detail. The model proposed for the overall kinetics has been verified by means of linear and nonlinear fittings up to the millisecond range. The identification of the intermediates has been based on ab initio optimized production enthalpies, as well as on the comparison of semiempirically predicted electronic transitions with the spectra observed after pulse radiolysis. The radical attack produces a radical adduct to the ring in position 5, $k = (4.7 \pm 0.8) \times 10^9$ M^{-1} s^{-1}, which in sequence undergoes first a β-cleavage, $k = (4.7 \pm 2.4) \times 10^5$ s^{-1}, and then a 1−6 hydrogen transfer, $k = (3.4 \pm 1.3) \times 10^4$ s^{-1}. The final decay to a very low absorbing molecule occurs through a second-order reaction, $k = (3.0 \pm 0.5) \times 10^8$ M^{-1} s^{-1}.

Introduction

A synthetic compound derived from furfural and sorbitol (sorbitylfurfural) has been recently exploited in the cosmetic industry as a skin-protecting agent. This activity is in connection with its antioxidant properties toward damaging radicals naturally present in the atmosphere, like OH, H, $O_2^{\bullet-}$, etc. In this context we undertook a thorough investigation on the oxidation of sorbitylfurfural and its separate components due to the OH radicals. The present paper is part of this study and deals with the mechanism of OH attack on furfural in water at natural pH. Furfural (2-furaldehyde or furan-2-carboxyaldehyde) is a well-known natural compound,[1] used extensively in the vegetable oil, petroleum, plastics, and rubber industries. It is produced from agricultural wastes containing pentosan via dehydration with acids. Its use as a viable plant-derived biochemical alternative to petrochemicals is being explored, in the attempt to reduce pollution. Nevertheless, furfural is also a pollutant agent: the combustion of wood material and other biomass causes the dispersion of aromatic carbonyl compounds among which the presence of furfural has been reported. Some recent studies[2] claim that, under the action of light, furfural participates in an atmospheric cycle which leads to the final production of hydrogen peroxide, a known precursor of acid pollutants.

Spectroscopic and kinetic data on the OH-induced degradation of furfural are scanty in the literature. An intermediate structure has been identified by Schuler[3] et al. on the basis of the ESR spectrum of electron-irradiated furfural in aqueous solution, indicating the opening of the furanic ring following OH addition in basic solution. A similar mechanism had been proposed previously by Lilie[4] in a pulse radiolysis study of furan in aqueous alkaline solution. A few kinetic data from competitive methods were reported by Savel'eva[5] and Vysotskaya[6] on γ-radiolysis, but no characterization of the processes and of the transients involved was given. The nature and destiny of the intermediates formed upon reaction of OH with furfural is the subject of the present paper. As the energetics of OH attack and of ring opening had not been investigated, we decided to compute the enthalpies of various reaction paths and to verify whether the electronic transitions of the intermediates could fit the observed UV−vis spectra. The kinetic traces were then submitted to a nonlinear fitting routine from which rate constants and extinction coefficients have been derived.

Materials and Methods

Furfural (Fluka puriss) was used as received. Solutions were prepared with Millipore (Milli-Q) water, purged with argon, and then saturated with N_2O. The natural pH of the system was 6.7.

Pulse radiolysis experiments were performed by using the 12 MeV linear accelerator (Linac) at the FRAE Institute.[7] Details on the optical detection system, methods, and computer treatment of data are described elsewhere.[8] Pulses of 10−50 ns delivering doses from 3 to 70 Gy were used. The radiation dose per pulse was monitored by means of a charge collector plate calibrated with an O_2-saturated solution of 0.1 M KSCN and by taking $G\epsilon_{500\ nm} = 2.15 \times 10^4$ $(100\ eV)^{-1}$ M^{-1} cm^{-1}, where G and ϵ are respectively the usual radiation yield and extinction coefficient for the $(SCN)_2^{\bullet-}$ radical. Absorption spectra of nonirradiated solutions were recorded with a Perkin-Elmer Lambda 9 spectrophotometer.

Geometry optimizations of radicals and stable products were performed by using the Gaussian94[9] on a Digital Alpha AXP 3000/500, at the HF level, utilizing a 3-21G* basis. The optimized geometries were then used in semiempirical excited-state computations based on the ZINDO/S Hamiltonian[10] yielding excitation energies and oscillator strengths. Finally, the spectral data thus obtained were convoluted to output a qualitative representation of the UV−vis spectrum for each species considered; a Lorentzian expression was used to calculate, for each transition, the intensity of the bands, which were then summed up to yield the spectrum.[11] The electronic transitions of furfural itself were computed as a first step to

* To whom correspondence should be addressed. Tel.: +39 0516399774. Fax: + 39 0516399844. E-mail: emmi@frae.bo.cnr.it.
[†] FRAE.
[‡] Università di Bologna.

10.1021/jp983883d CCC: $18.00
Published on Web 01/28/1999

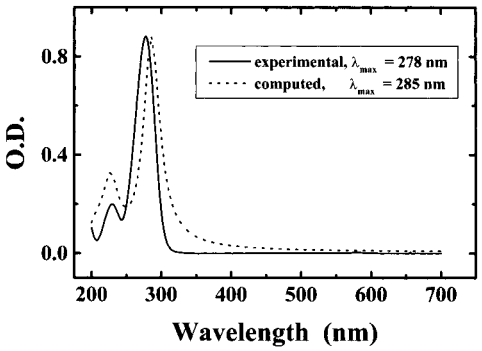

Figure 1. Comparison of experimental and computed spectra of furfural ([furfural] = 6.03×10^{-4} M; optical path = 0.1 cm). Computed data are normalized to the experimental maximum of absorbance.

verify the reliability of the semiempirical method.[12] Their values were convoluted to reproduce the spectrum in Figure 1. The agreement between experimental and computed bands supports the further application of the method to the furfural-derived species.

Linear-fitting was used to test if the behavior of optical densities vs time can be interpreted by simple kinetic models by using two programs developed in Asyst language.[13]

Nonlinear (curve) fitting was carried out by using the Facsimile chemical modeling package.[14] It uses numerical techniques and a special high-level programming language in which chemical reactions are expressed as ordinary differential equations. Facsimile contains a parameter-fitting option, whereby specified parameters can be adjusted with a recursive calculation to minimize the sum of the squares of all the residuals for all the data. For a numerical evaluation of the fitting quality the usual reduced-χ^2 parameter[15] is reported in the legends of the figures.

Results and Discussion

1. Pulse Radiolysis. Furfural in concentrations ranging from 1.2×10^{-4} to 1.8×10^{-3} M was investigated by pulse radiolysis of N_2O-saturated aqueous solution at natural pH, thus converting aqueous electrons into OH. At natural pH the concentration ratio of the resulting radicals was considered to be 91% of OH and 9% of H (G(OH) = 5.8 and G(H) = 0.55). The reactions of H atoms are usually close to those of OH[16] and will not be specifically considered in this paper.

After irradiation an increase of optical density is observed in the UV−vis region, with intensity peaks centered at 245, 315, 400, 440, and 560 nm, as shown in Figure 2. Between 250 and 300 nm a blind zone is present where furfural itself absorbs. Therefore, partial observations in this area can be made only in very diluted samples. The intensities at 315 and 440 nm increase up to 5 μs and then decrease, while in the same time frame the peaks at 400 and 560 nm increase continuously. An isosbestic point can be observed around 350 nm in the time frame between 5 and 45 μs (see inset in Figure 2), indicating that a conversion of a species into another is taking place.

The optical density changes at the two more prominent peaks are illustrated in Figure 3 (λ = 315 nm) and Figure 4 (λ = 400 nm). Similar behavior is presented at 440 and 560 nm, respectively. Absorbance changes vs time are similar at all concentrations and irradiation doses used.

By examination of the spectra (Figure 2) and kinetics (Figures 3 and 4), a series of consecutive processes can be recognized which can be schematically drawn as follows. At [furfural] = 0.12 mM the OH attack goes to completion within 5 μs, producing one or more intermediates with peak absorptions at 315 and 400 nm, with a 4:1 ratio. Thereafter the absorption increases at 400 nm and decreases at 315 nm; i.e., these intermediates are transformed into other species which, although absorbing in the same region, cause a reduction in the ratio above. Further reactions then lead to bleach the spectrum in the millisecond time range, leaving a weak residual absorption.

Three approaches—linear-fitting, ab initio optimization followed by semiempirical computation of spectra and comparison with the experimental ones, and curve-fitting—have then been applied in order to unravel the kinetics and to conjecture a mechanism.

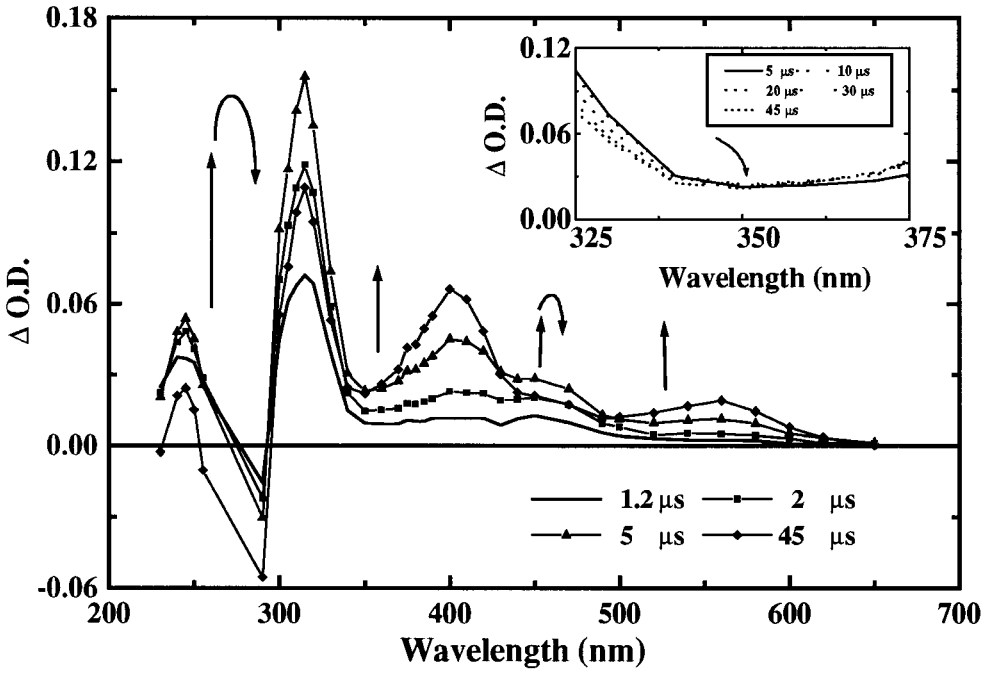

Figure 2. Time-resolved spectra after pulse radiolysis of 1.2×10^{-4} M furfural in an N_2O-saturated solution at natural pH. Curved arrows indicate a bleaching after an absorbance growth. Dose = 17 Gy, pulse length = 20 ns, and optical path = 5 cm. Inset: enlargement of the isosbestic point region, spectra selected from 5 to 45 μs after the pulse.

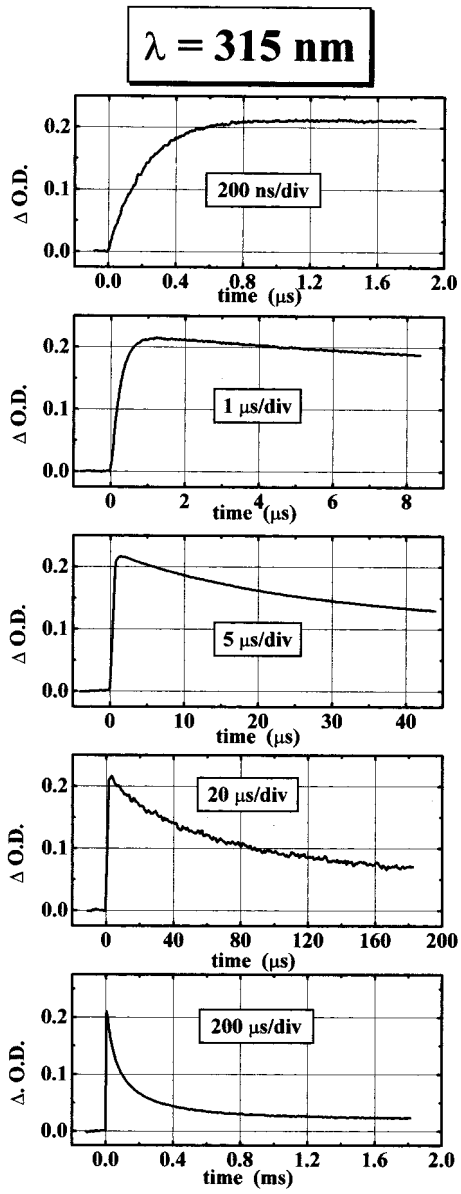

Figure 3. Sequence at different time scales of the processes observed at 315 nm and natural pH, with dose = 18 Gy, optical path = 5 cm, and [furfural] = 6.03×10^{-4} M.

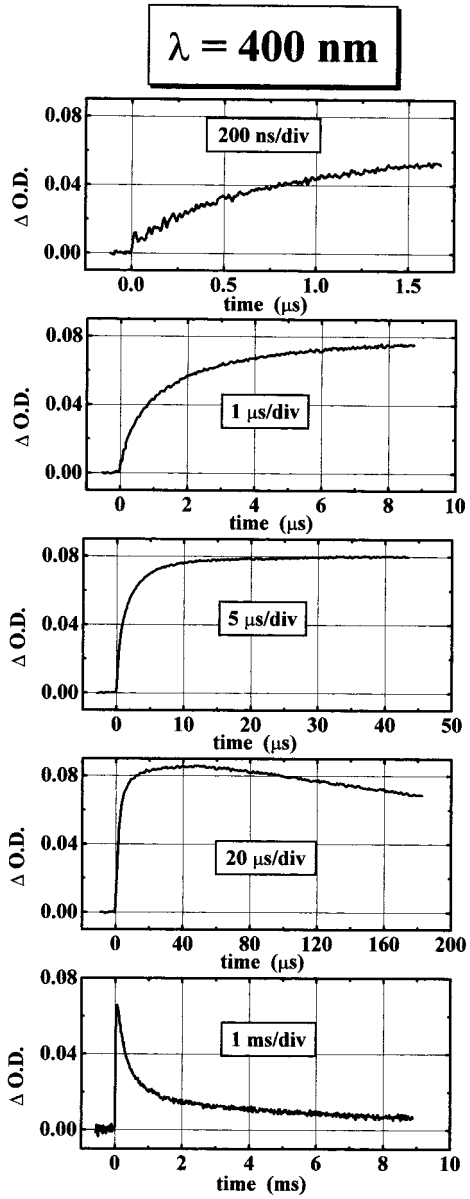

Figure 4. Sequence at different time scales of the processes observed at 400 nm and natural pH, with dose = 18 Gy, optical path = 5 cm, and [furfural] = 6.03×10^{-4} M for all the traces except at 1 ms/div, for which dose = 17 Gy and concentration = 1.2×10^{-4} M.

2. OH Attack and Species Identification. The observed formation rate constant varies linearly with furfural concentration at 315 nm but not at 400 nm; in fact, here linearity is broken when furfural exceeds 1.3 mM. Therefore a linear fitting produces two different buildup rate constants at two different wavelengths. This discrepancy suggests that the observation of the OH attack is entangled by the instability of the products. Actually, by comparison of the corresponding curves of Figures 3 (315 nm) and 4 (400 nm) on the scale of 20 μs/div, it should be remarked that, while the product decays plainly at 315 nm, it grows in a more-than-one-step behavior and then decays at 400 nm. Hence, OH-induced degradation of furfural follows a more complex kinetics. As reported in earlier studies on the furanic ring,[3,4] OH attack is followed by consecutive rearrangements of the derived radical, which afterward finally decays.

About the possible attack paths, dealing with aliphatic[17−19] and aromatic[20,21] aldehydes and furanic[3−6,22] compounds, the literature reports three possible routes which, in the order, can produce either an adduct radical, an acylic radical, or a radical cation.

Even though an adduct in position 5 was identified by ESR spectra on a series of furanic rings,[3] we tried to rationalize hypotheses and observations by studying in detail the energetics of the above reactions.

In principle five adducts can be produced: **IA-2**, **IA-3**, **IA-4**, **IA-5**, or **IA-6** (Chart 1). The acylic radical **IB**[23] is expected to show an absorption maximum at ca. 315 nm as it was reported for an analogous species (derived from C_6H_5COCl)[24] and a very weak absorption at 400 nm.[25,26] Finally, an electron transfer can produce the radical cation **IC**, as proposed by Shiga and Isomoto.[22]

The ab initio optimization of the structures of Chart 1 leads to the values of the sum of electronic and thermal enthalpy (SETE) reported in Table 1. These values were used to calculate the enthalpies of the reactions in which each species is produced, by applying the usual Hess's law.

As expected,[3−6] attack in position 5 (**IA-5**), producing a resonant allylic radical on carbons C2, C3, and C4 (see Chart 1), turns out to be more exothermic than any other path by 14

TABLE 1: Enthalpic Parameters and Electronic Transitions Concerning the OH Addition Step

reagents and products	SETE[a] (au)	production enthalpy (kcal/mol)	calcd electronic transitions (nm)
furfural	−339.349 8		225, 285
H_2	−1.106 848		
OH	−74.958 703		
H_2O	−75.560 416		
OH^-	−74.858 678		
IA-2	−414.337 811	−18.4	277, 294
IA-3	−414.328 772	−12.7	280, 332
IA-4	−414.303 597	+3.1	266, 314
IA-5	−414.360 572	−32.7	313, 331, 422, 479, 544
IA-6	−414.332 431	−15.0	221, 261
IB	−338.740 535	+4.7	300
IC	−339.058 604	+245.5	311, 600

[a] SETE: sum of electronic and thermal enthalpies for optimized structures.

CHART 1

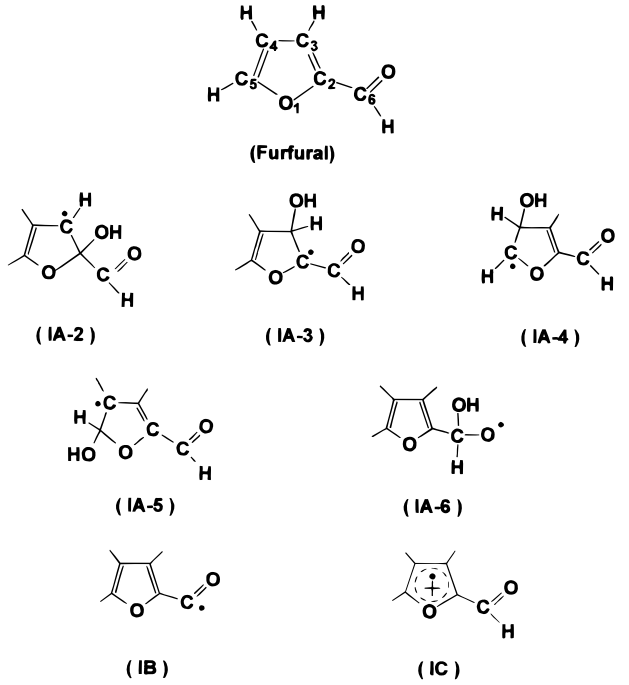

kcal/mol. The spectral data are also reported in Table 1. Radical **IA-5** is the sole radical showing electronic transitions located in the UV as well as in the visible region, thus satisfying the expectations from the pulse radiolysis spectrum.

The acylic radical (**IB**) and the radical cation (**IC**) can be ignored, since besides lacking absorption at 400 nm their production could be justified only if a large entropy change could balance an unfavorable enthalpy. The production of an amount of acylic radical cannot be excluded, but its quantitative contribution should be so little as to become negligible. The expectation that **IA-5** is the intermediate of choice finds then new basis of support.

3. Processes Involving the OH Adduct. Adduct **IA-5** does not dimerize but disappears via a first-order process. Three tentative examples of monomolecular rearrangements are reported in Scheme 1, two of which—water and hydrogen elimination—are usually considered very unusual or not possible. However their reaction enthalpies have been calculated in view of the extended conjugation presented byproducts **IIIA** and **IIIB**, respectively. Ring opening (**IIIC**) is reported to be entropically favored,[27] and when accompanied by the formation

SCHEME 1

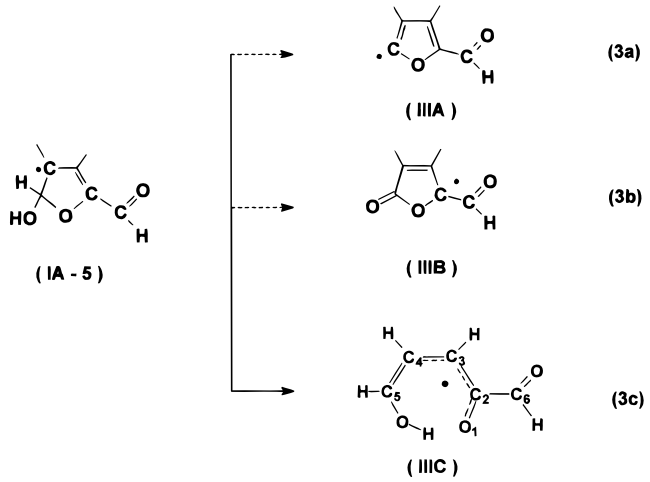

SCHEME 2

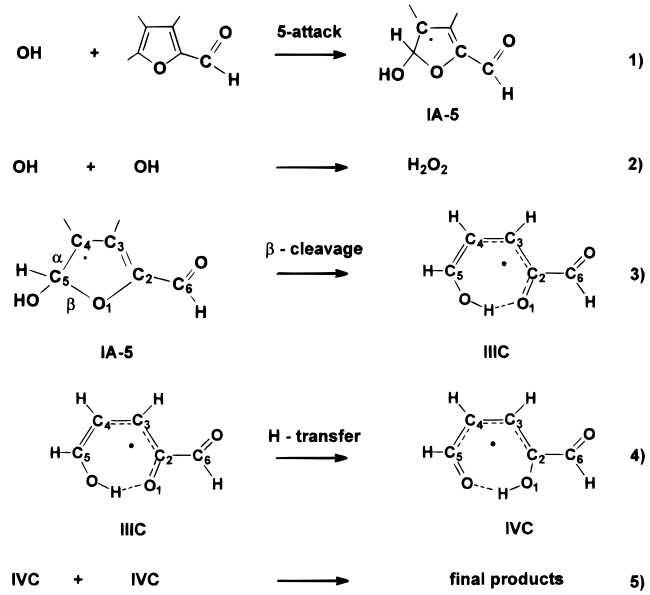

TABLE 2: Enthalpic Parameters and Electronic Transitions Concerning the Possible Products of IA-5 Transformation

species	SETE[a] (au)	production enthalpy (kcal/mol)	calcd electronic transitions (nm)	exptl bands (nm)
IIIA	−338.721 308	+49.5	376	
IIIB	−413.244 658	+5.7	297, 429, 519	
IIIC	−414.363 294	−1.7	307, 395, 565	300, 400, 450, 570

[a] SETE: sum of electronic and thermal enthalpies of optimized structures.

of a new carbonyl group, it occurs even if the transformation is expected to be endothermic. The above mentioned studies[3,4] moreover identified a similar structure at alkaline pH. On that account, cleavage in β-position is generally accepted (Scheme 2), although, in some cases, a rearrangement through α-cleavage has also been pointed out.[28] Actually this path entails the formation of an intermediate carbene structure localized on carbon C4, an event that requires a substantially high enthalpy, which ab initio calculations assessed as $\Delta H = 63.9$ kcal/mol. Thus α-cleavage will not be taken in consideration any further.

The data reported in Table 2 show that while deaquation (formation of **IIIA)** and hydrogen elimination (formation of **IIIB)** are endothermic to a different extent, β-cleavage (forma-

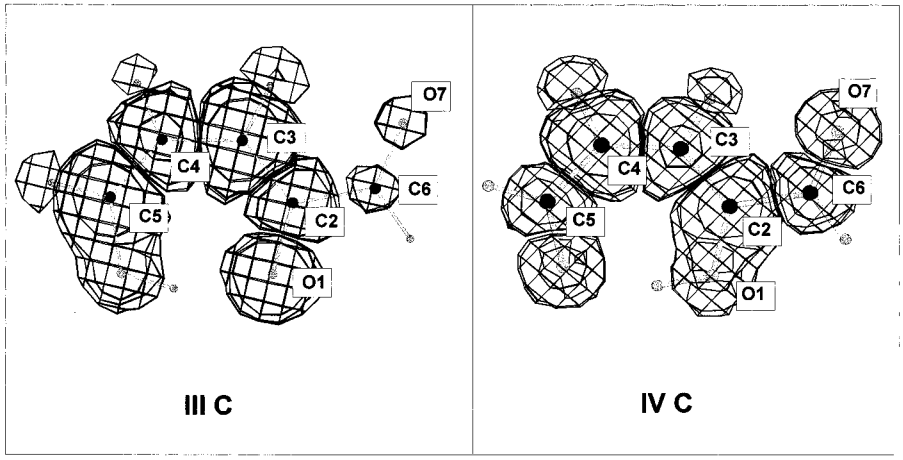

Figure 5. Spin density distribution of the intermediate radicals **IIIC** and **IVC** formed in the degradation of the OH adduct of furfural after pulse radiolysis in aqueous solution at natural pH.

tion of **IIIC)** is a slightly exothermic process. However, this process is found to be exothermic only if it forms a structure where the OH attacking group is directed toward the furanic oxygen O1 (*syn*-orientation). On the contrary, if the OH group and O1 are in *anti*-orientation, the process results endothermic by 9.3 kcal/mol. The driving force in the former case could be the gain of stability supplied by the formation of a H-bond between the OH attacking group and O1. Such an H-bond has been predicted in the optimized structure of **IIIC**, as the distance between H and O1 is shorter than 3.2 Å and the angle O−H−O is higher than 150° (the values found in our case are 1.76 Å and 155.5°, respectively). In the OH adduct (**IA-5**) conjugation in the π-system is reduced because carbon C5 becomes tetrahedral; however, following C5−O1 bond breaking, the formation of an H-bond helps radical **IIIC** to find a new planar arrangement in a pseudo-7-atom-ring which allows, again, a large conjugation of π electrons. Last but not least, this configuration appears to be the necessary intermediate to allow a further rearrangement into an even more stable radical (**IVC)** (Figure 5) where conjugation is extended to the aldehyde group. This occurs, in fact, with a production enthalpy equal to −6.5 kcal/mol, via a 1−6 oxygen−oxygen H-transfer and the formation of a new carbonyl bond (C5═O) (reaction 4/Scheme 2). The above considerations apply at near neutral pH, while in alkaline solutions the mechanism can also proceed through the formation of an anionic intermediate.[3,4]

4. Spectra. The correspondence of many of the electronic transitions predicted for **IIIC** with most of the experimental bands prompted us to attempt a detailed spectral verification of its presence among the reaction components.

As the rapid transformation undertaken by the radical prevents the isolation of its spectral contribution, we simulated the pulse radiolysis spectra obtained at the two key times of 1.2 and 5 μs (Figure 2) by making use of the calculated transitions of both **IA-5** and **IIIC**, of their oscillator strengths, and of their relative concentrations as calculated by curve fitting data (see next section).

The elapsed time of 1.2 μs represents that stage of the process when the hydroxylated radical **IA-5** is mostly responsible for the 315 and 400 nm peaks. Its computed optical contribution, normalized to the experimental intensity of the 315 nm peak, is shown in Figure 6a.

At the second key time of 5 μs, the 315 nm absorption reaches its maximum intensity, while the 400 nm band is still growing: the radical attack went to completion and, besides the adduct **IA-5**, radical **IIIC** is present as well.

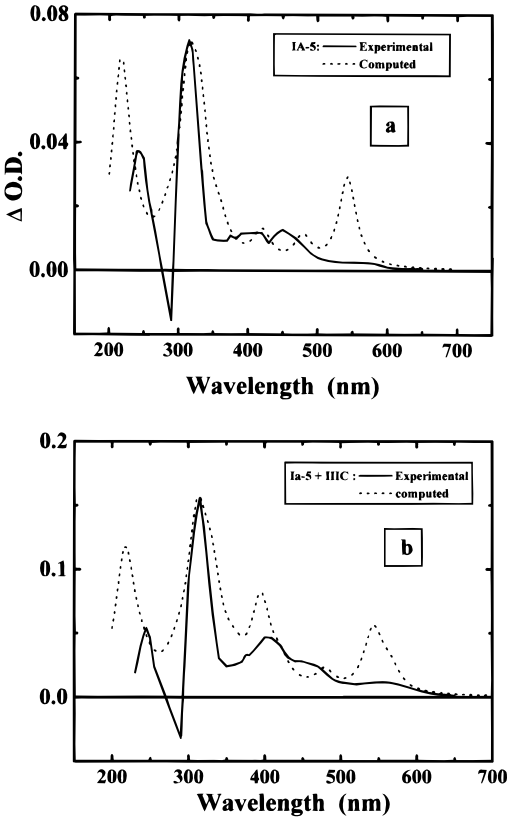

Figure 6. Comparison of experimental and computed spectrum of pulse irradiated furfural ([furfural] = 1.2×10^{-4} M; N_2O-saturated solution; natural pH; dose = 17 Gy; pulse length = 20 ns; optical path = 5 cm). Computed absorptions were normalized to the experimental maximum. (a) Experimental spectrum recorded 1.2 μs after the pulse. (b) Experimental spectrum recorded 5 μs after the pulse. Each computed absorbance contribution accounts for the concentration of the species calculated with the parameters listed in Table 3.

The sum of the convoluted spectral contributions of **IIIC** and **IA-5** (Figure 6b) appears to describe satisfactorily the experimental spectrum, reproducing the position of the five main bands at both times. The agreement of the simulated spectra is also remarkable from the dynamic point of view, since from Figure 6a (1.2 μs) to Figure 6b (5 μs) the ratio A_{315}:A_{400} diminishes, as it actually occurs experimentally (see section 1).

5. Curve Fitting. The proposed kinetic model reported in Scheme 2, has been submitted to a curve-fitting procedure. The fitting was performed at the two most representative wavelengths

TABLE 3: Optimized Kinetic Constants and Extinction Coefficients[a]

kinetic constants	ϵ at 315 nm (M^{-1} cm^{-1})	ϵ at 400 nm (M^{-1} cm^{-1})
$k_1 =$ $(4.7 \pm 0.8) \times 10^9$ M^{-1} s^{-1}	**IA-5**: 6220 ± 393	**IA-5**: 648 ± 95
$k_2 =$ 5.5×10^9 M^{-1} s^{-1} (ref 29)		
$k_3 =$ $(4.7 \pm 2.4) \times 10^5$ s^{-1}	**IIIC**: 4210 ± 328	**IIIC**: 1370 ± 111
$k_4 =$ $(3.4 \pm 1.3) \times 10^4$ s^{-1}	**IVC**: 2320 ± 372	**IVC**: 1740 ± 160
$k_5 =$ $(3.0 \pm 0.5) \times 10^8$ M^{-1} s^{-1}	final product: 880 ± 250	final product: 370 ± 130

[a] Error limits represent two standard deviations.

(315 and 400 nm), for different concentrations (0.12−1.8 mM) and doses (10−70 Gy).

The sole fixed values were the OH recombination rate constant $k_2 = 5.5 \times 10^9$ M^{-1} s^{-1} [29] and the extinction coefficient of furfural, $\epsilon_{315} = 265$ M^{-1} cm^{-1} and $\epsilon_{400} = 0$ M^{-1} cm^{-1}. All the other kinetic and spectral parameters were optimized to obtain the best fit. The average values of these parameters are summarized in Table 3. As representative examples, various fittings are illustrated in Figure 7. While plots 7a,b represent the core of the kinetic process at two different concentrations and wavelengths, plot 7c shows the final decay of the radical species at higher dose rate and concentration.

It is highly remarkable that two first-order reactions (reactions 3 and 4) and a second order (reaction 5) in sequence are necessary to allow the iterative nonlinear fitting to reach a consistent and homogeneous minimization of errors. On the contrary we verified that models differing from Scheme 2 could not match the parameters at two different wavelengths or concentrations or doses. If reaction 4—H-transfer—is removed from the model, the quality of fitting is greatly reduced and the χ^2 value gets 100-fold worse.

The rate constant value found for ring opening at pH 6.7, $k_3 = (4.7 \pm 2.4) \times 10^5$ s^{-1}, is somewhat lower than that reported by Lilie[4] for furan, but the latter has been evaluated in alkaline solution where the cleavage seems to proceed through an intermediate anionic species.

Conclusions

The nature and fate of the radicals produced in the pulse radiolysis of aqueous solutions of furfural at natural pH were investigated by combining transient absorption spectra and kinetics with various computation methods: linear and nonlinear kinetic fittings, ab initio computed reaction enthalpies, semiempirical computed electronic transitions, and simulation of transient spectra. A nonlinear fitting, used recursively until the kinetic parameters were consistent with each other at various wavelengths, concentrations, and doses, discloses that linear fitting is inadequate to describe the sequence of rapid transformations undergone by the OH adduct. A negative enthalpy of reaction, larger than that leading to any other adduct or electron-transfer product, favors the formation of a 5-hydroxylated radical (**IA-5**), confirming previous reports. The simulated spectrum of **IA-5** is also in agreement with this conclusion, and if reaction branching occurs, it seems to be limited to a very low extent. The 5-hydroxylated radical suffers, then, a ring bond breaking (β-cleavage); its product is a planar conjugated radical (**IIIC**), characterized by a spin density almost equally distributed along the O1−C2−C3−C4−C5 skeleton (Figure 5). Its calculated electronic transitions match the experimental absorbance bands,

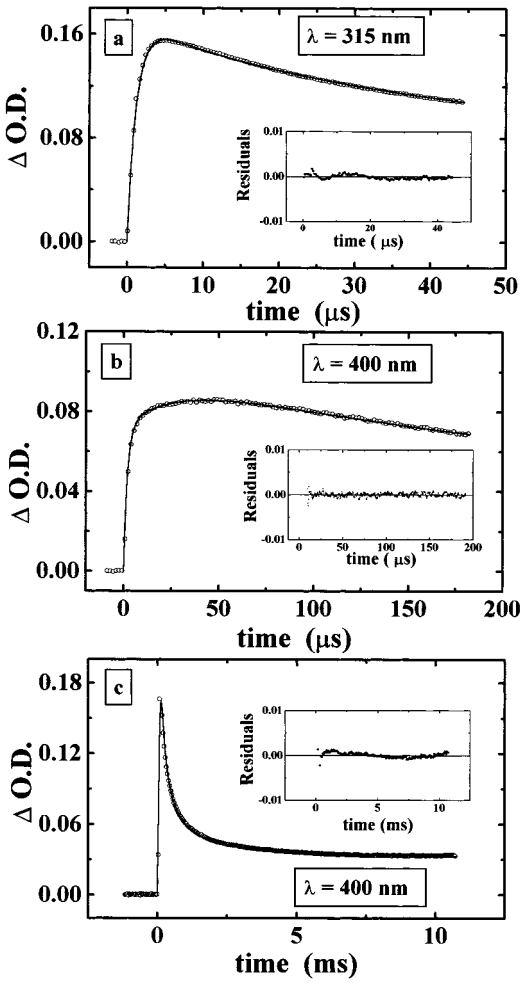

Figure 7. Output of the best fittings of the reaction model reported in Scheme 2: (a) [furfural] = 1.2×10^{-4} M, $\lambda = 315$ nm, dose = 17 Gy, optical path = 5 cm, goodness of fitting $\chi^2 = 1.97 \times 10^{-5}$; (b) [furfural] = 6.03×10^{-4} M, $\lambda = 400$ nm, dose = 18 Gy, optical path = 5 cm, goodness of fitting $\chi^2 = 2.52 \times 10^{-6}$; (c) [furfural] = 1.08×10^{-3} M, $\lambda = 400$ nm, dose = 70 Gy, optical path = 5 cm, goodness of fitting $\chi^2 = 1.44 \times 10^{-5}$. Insets: diagram of residuals.

and its structure is such as to facilitate a 1−6 hydrogen transfer mediated by H-bonding. A rearrangement into a new radical (**IVC**), which leads to a wider spin delocalization extending over the aldehyde group (Figure 5), is thus likely to occur. In fact, it has been found that such a rearrangement is exothermic and fits the complex experimental absorption curves. Then its final destiny appears to be the transformation into a low absorbing product via a neat second-order reaction. At the present stage of the work it cannot be said if the nature of this process is a dimerization or a disproportionation.

Acknowledgment. Sincere thanks are due to Dr. C. Chatgilialoglu for his valuable comments and suggestions concerning this work. We are obliged to Dr. V. Bertelli of Laboratori Fitocosmesi e Farmaceutici srl (Milano, Italy) who kindled our interest to the antioxidant properties of furfural derivatives. The skillful assistance of A. Monti with the pulse radiolysis equipment and of R. Cortesi with a wide range of computers is highly appreciated.

References and Notes

(1) (a) Sammes, P. G. *Comprehensive Organic Chemistry, Volume 4 Heterocyclic Compounds*; Barton, D., Ollis, W. D., Eds.; Pergamon Press:

London, 1979; p 732. (b) Fieser, L. F.; Fieser, M. *Organic Chemistry*, 3rd ed.; Reinhold Publishing Corp.: London, 1956; pp 866−870. (c) Roberts J. D.; Caserio, M. C. *Basic Principles of Organic Chemistry*; W. A. Benjamin Inc.: New York, 1964; Chapter 18, p 27.

(2) Anastasio, C.; Faust, B. C.; Rao, C. J. *Environ. Sci. Technol.* **1997**, *31*, 218−232.

(3) Schuler, R. H.; Laroff, G. P.; Fessenden R. W. *J. Phys. Chem.* **1973**, *77*, 456−466.

(4) Lilie, J. *Z. Naturforsch.* **1971**, *26b*, 197−202.

(5) Savel'eva, O. S.; Shevchuk, L. G.; Vysotskaya, N. A. *J. Org. Chem USSR* **1973**, *9*, 759−761.

(6) Vysotskaya, N. A.; Shevchuk, L. G.; Gavrilova, S. P.; Badovskaya, L. A.; Kul'nevich, V. G. *J. Org. Chem USSR* **1983**, *19*, 1352−1354.

(7) Hutton, A.; Roffi, G.; Martelli, A. *Quad. Area Ric. Emilia-Romagna* **1974**, *5*, 67−74.

(8) Emmi, S. S.; D'Angelantonio, M.; Poggi, G.; Beggiato, G.; Camaioni, N.; Geri, A.; Martelli, A.; Pietropaolo, D.; Zotti, G. *Res. Chem. Intermed.* **1998**, *24*, 1−14.

(9) Frisch, M. J.; Trucks, G. W.; Schlegel, H. B.; Gill, P. M. W.; Johnson, B. G.; Robb, M. A.; Cheeseman, J. R.; Keith, T. A.; Petersson, G. A.; Montgomery, J. A.; Raghavachari, K.; Al-Laham, M. A.; Zakrzewski, V. G.; Ortiz, J. V.; Foresman, J. B.; Cioslowski, J.; Stefanov, B. B.; Nanayakkara, A.; Challacombe, M.; Peng, C. Y.; Ayala, P. Y.; Chen, W.; Wong, M. W.; Andres, J. L.; Replogle, E. S.; Gomperts, R.; Martin, R. L.; Fox, D. J.; Binkley, J. S.; Defrees, D. J., Baker, J.; Stewart, J. P.; Head-Gordon, M.; Gonzales, C.; Pople, J. A. *Gaussian94 Rev. C.3*; Gaussian, Inc.: Pittsburgh, PA, 1995.

(10) HyperChem, Rel 5 for Windows. *Molecular Modeling Systems*; Hypercube Inc.: Waterloo, Ontario, Canada, 1996.

(11) *Microcal Origin, V. 5.00*; Microcal Software Inc.: Northampton, MA, 1997.

(12) Del Bene, J.; Jaffe, H. H. *J. Chem. Phys.* **1968**, *48*, 4050−4055.

(13) (a) Camaioni, N.; Mulazzani Q. *Technical Report 8/93*; Istituto FRAE-CNR: Bologna, Italy, 1993. (b) Camaioni, N.; Emmi, S. S.; Mulazzani, Q. *Technical Report 9/93, V. 1.0*; Istituto FRAE-CNR: Bologna, Italy, 1993.

(14) *FACSIMILE V. 3.0, Process and chemical reaction modeller, User Guide and Technical Reference*; Aea Industrial Technology, Harwell Laboratory, UKAEA: Harwell, Didcot, Oxfordshire, U.K., 1993.

(15) Box, G. E. P.; Hunter, W. G.; Hunter, J. S. *Statistics for Experimenters. An Introduction to Design, Data Analysis, and Model Building*; J. Wiley and Sons, Inc.: New York, 1978; Chapter 6.

(16) Swallow, A. J. *Radiation Chemistry An Introduction*; Longman Group Limited: London, 1973; p 153.

(17) Dobe, S.; Khachatryan, L. A.; Berces, T. *Ber. Bunsen-Ges. Phys. Chem.* **1989**, *93*, 847−852.

(18) Schuschmann, M. N.; von Sonntag, C. *J. Am. Chem. Soc.* **1988**, *110*, 5698−5701.

(19) Santiard, D.; Sabourault, D.; Ribiere, C.; Nordmann, R.; Houee-Levin, C.; Ferradini, C. *J. Chim. Phys.* **1991**, *88*, 967−976.

(20) Matus, I.; Kroo E.; Putirskaya G. V. *The Interaction of OH Radicals with Aromatic Alchools, Aldehydes, Hydroperoxides and Acids*; 5th Symposium on Radiation Chemistry; Publishing House of the Hungarian Academy of Science: Budapest, 1982; pp 263−270.

(21) Chutny, B. *Nature* **1967**, *11*, 593−594.

(22) Shiga, T.; Isomoto, A. *J. Phys. Chem.* **1969**, *73*, 1139−1143.

(23) Chatgilialoglu, C.; Lunazzi, L.; Macciantelli, D.; Placucci, G. *J. Am. Chem. Soc.* **1984**, *106*, 5252−5256 and references therein reported.

(24) Noda, S.; Fueki, K.; Kuri, Z. *J. Chem. Phys.* **1968**, *49*, 3287−3292.

(25) Chatgilialoglu, C.; Ingold, K. U.; Scaiano, J. C.; Woynar H. *J. Am. Chem. Soc.* **1981**, *103*, 3231−3232.

(26) Huggenberger, C.; Lipscher, J., Fischer, H. *J. Phys. Chem.* **1990**, *84*, 3467−3474.

(27) Wilt, J. W. *Free Radicals*; Kochi, J. K., Ed.; J. Wiley and Sons: New York, 1973; Vol. I, p 413.

(28) Ingold, K. U. *Free Radicals*; Kochi, J. K., Ed.; J. Wiley and Sons: New York, 1973; Vol. I, p 99.

(29) Buxton, G. V.; Greenstock, C. L.; Helman, W. P.; Ross A. B. *J. Phys. Chem. Ref. Data* **1988**, *17*, 513−886.